

SMALL-SCALE PROPERTIES OF ATOMIC GAS IN EXTENDED DISKS OF GALAXIES

SANCHAYEETA BORTHAKUR

Department of Physics and Astronomy, Johns Hopkins University, Baltimore, MD 21218, USA

EMMANUEL MOMJIAN

National Radio Astronomy Observatory, Socorro, NM, USA

TIMOTHY M. HECKMAN

Department of Physics and Astronomy, Johns Hopkins University, Baltimore, MD 21218, USA

DONALD G. YORK

Department of Astronomy and Astrophysics, University of Chicago, Chicago, IL 60637, USA; Enrico Fermi Institute, University of Chicago, Chicago, IL 60637, USA

DAVID V. BOWEN

Princeton University Observatory, Peyton Hall, Ivy Lane, Princeton NJ 08544

MIN S. YUN

Astronomy Department, University of Massachusetts, Amherst, MA 01003, USA

TODD M. TRIPP

Department of Astronomy, University of Massachusetts, Amherst, MA 01003, USA

Draft version September 16, 2014

ABSTRACT

We present high-resolution H I 21 cm observations with the Karl G. Jansky Very Large Array (VLA) for three H I rich galaxies in absorption against radio quasars. Our sample contains six sightlines with impact parameters from 2.6 to 32.4 kpc. We detected a narrow H I absorber of FWHM 1.1 km s^{-1} at 444.5 km s^{-1} towards J122106.854+454852.16 probing the dwarf galaxy UCG 7408 at an impact parameter of 2.8 kpc. The absorption feature was barely resolved and its width corresponds to a maximum kinetic temperature, $T_k \approx 26 \text{ K}$. We estimate a limiting peak optical depth of 1.37 and a column density of $6 \times 10^{19} \text{ cm}^{-2}$. The physical extent of the absorber is 0.04 kpc^2 and covers $\sim 25\text{--}30\%$ of the background source. A comparison between the emission and absorption strengths suggests the cold-to-total H I column density in the absorber is $\sim 30\%$. Folding in the covering fraction, the cold-to-total H I mass is $\sim 10\%$. This suggest that condensation of warm H I ($T_s \sim 1000 \text{ K}$) to cold phase ($T_s < 100 \text{ K}$) is suppressed in UGC 7408. The unusually low temperature of the H I absorber also indicates inefficiency in condensation of atomic gas into molecular gas. The suppression in condensation is likely to be the result of low-metal content in this galaxy. The same process might explain the low efficiency of star formation in dwarf galaxies despite their huge of gas reservoirs. We also report the non-detection of H I in absorption in five other sightlines. This indicates that either the cold gas distribution is highly patchy or the gas is much warmer ($T_s > 1000 \text{ K}$) towards these sightlines.

Subject headings: galaxies: abundances — galaxies: ISM — quasars: absorption lines

1. INTRODUCTION

The accretion and subsequent condensation of inflowing ionized gas, with temperatures of 10^4 to 10^6 K , from the intergalactic medium (IGM) and circumgalactic medium (CGM) into the interstellar medium (ISM) of galaxies, with temperatures of 10^2 to 10^4 K , is a crucial aspect of the baryon cycle. While our theoretical understanding of gas inflow into galactic halos has progressed tremendously in the last couple of decades (including work by Birnboim & Dekel 2003; Maller & Bullock 2004;

Kereš et al. 2005; Ford et al. 2013), the processes that enable the gas to actually condense and achieve physical conditions where stars can form are not yet well understood. On the observational front, several studies have confirmed the presence of vast reservoirs of cool gas ($10^9 M_\odot$ of gas at $10^{4\text{--}5} \text{ K}$; Werk et al. 2014) and metals (Wakker & Savage 2009; Prochaska et al. 2011; Tumlinson et al. 2011; Borthakur et al. 2013; Bordoloi et al. 2014) in the CGM of galaxies of all types. Several studies have found correlations between the kinematics of cooler and hotter CGM gas phases (Tripp et al. 2008, 2011; Meiring et al. 2013). Similarly,

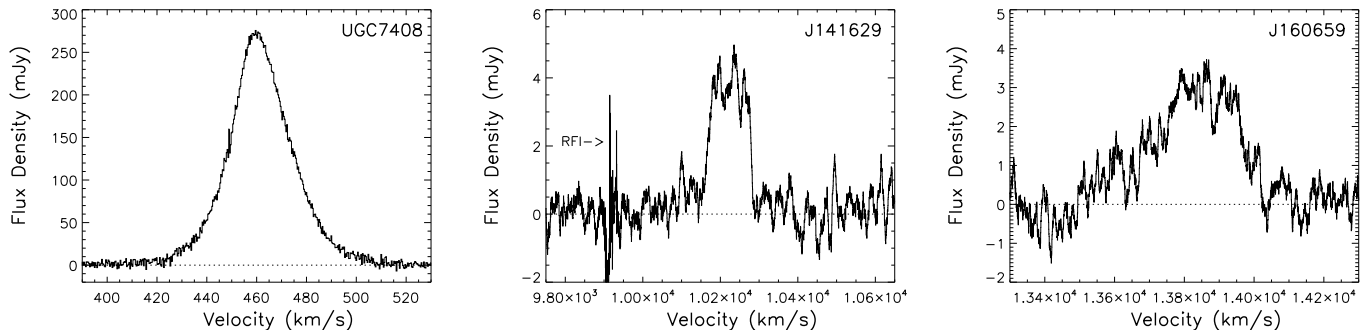


FIG. 1.— GBT HI spectra towards background quasars probing three foreground galaxies from the survey by B11. The GBT beam covered the quasar sightline along with the foreground galaxy. The spectra show strong HI emission features believed to be associated with the ISM of the foreground galaxy. The spectra towards quasar J122106+454852 probing galaxy UGC 7408 shows the data at original resolution. The spectra towards the other two sightlines probing galaxies J141629+372120 (labeled as J141629) and J160659+271642 (labeled as J160659) are smoothed by 30 pixels ($\equiv 10.6 \text{ km s}^{-1}$) to increase signal-to-noise ratio. No clear indication of 21cm HI absorption were seen in the raw or the smoothed data. The large GBT beam of FWHM $9''.1$ makes it impossible to interpret the physical significance of the non-detections of HI absorption towards these quasar sightlines. One explanation could be that there is an absence of gas in the region probed by the sightlines. However, it is also possible that 21 cm absorption produced towards the quasar sightlines are being filled-in by HI emission associated with gas elsewhere in the galaxies. Higher spatial resolution is warranted to distinguish between the two possible scenarios, thus our motivation for obtaining higher spatial resolution VLA observations.

TABLE 1
GALAXIES AND THEIR PROPERTIES.

Foreground Galaxy	Redshift	Stellar Mass (Log M_{\odot})	Metallicity ^a (12+log(O/H))	HI Mass (Log M_{\odot})	v_{HIpeak}^b (km s ⁻¹)	Δv_{HI}^c (km s ⁻¹)
J122115.22+454843.2 ^d	0.0015	7.4	8.3 ^e	8.3	460	417 - 507
J141629.25+372120.4	0.0341	9.3	8.6	9.4	10235	10070 - 10300
J160659.13+271642.6	0.0462	9.3	8.4	9.9	13860	13500 - 14030

^a Metallicity based on N2 index (Pettini & Pagel 2004). The metallicity was measured from emission lines from the central region of the galaxy and may be considered as the upper limit for the gas probed by the quasar sightlines.

^b Velocity corresponding to the peak of the HI profile.

^c Velocity width (full) of the emission profile.

^d Also known as UGC 7408.

^e Based on values published by Kennicutt et al. (2008).

evidence of extended cool rotating disks has been seen using probes such as Mg II absorbers (Steidel et al. 2002; Kacprzak et al. 2010).

Where does the infalling/circumgalactic gas condense into interstellar medium? How is that process regulated? And what do the properties of neutral gas in extended disks or extraplanar gas teach us about this process? In order to answer these questions and to understand the connection between the process of condensation and the properties of the ISM, detailed surveys of cold gas properties in the outer disks of galaxies are needed. For this purpose, H I 21 cm absorbers have been used by multiple teams to study properties of cold gas over a wide range of redshifts (e.g., Kanekar & Chengalur 1997; Lane & Briggs 2001; Vermeulen et al. 2003; Darling et al. 2004; Keeney et al. 2005; Gupta et al. 2007, 2009, 2010, 2013; Borthakur et al. 2010, 2011, and references therein).

In the last five years two low- z surveys by Gupta et al. (2010) and Borthakur et al. (2011, B11 hereafter) attempted a census of cold gas detection rate as a function of impact parameter from the host galaxy. These studies used radio-bright quasars to probe low- z galaxies at impact parameters ranging from 11-53 kpc and 2-100 kpc respectively. Due to rarity of small impact parameter quasar-galaxy pairs, the sample included a wide variety of galaxies with majority of them being sub-L*.

Despite the inhomogeneity in their galaxy properties, the two studies have provided independent estimation of covering fraction of cold gas to be $\approx 50\%$ within ~ 20 kpc. The detection of cold gas beyond that distance is exceedingly rare. However, it is worth noting that these surveys sparsely sampled the impact parameter range and did not take into account the effects of galaxy orientation. On the other hand, the number density and cross-section of Damped Lyman Alpha (DLA; i.e. absorbers with $N(\text{HI}) \geq 2 \times 10^{20} \text{ cm}^{-2}$) systems suggests a covering fraction of H I to be around 50% within 20 kpc of a galaxy (see Section 4.1 in B11; Section 6.1 in Schaye et al. 2007). Interestingly, the Milky Way's atomic gas disk with H I column densities to qualify as a DLA is about 20 kpc (Strasser et al. 2007; Kalberla & Kerp 2009, and references therein), although the disk extends to about twice that distance at much lower column densities (see Figure 8 Kalberla & Kerp 2009).

In this paper, we present follow-up observations of three of the galaxies from our previous H I absorption survey (B11). In our previous work, we reported nondetection of H I absorption in two of the targets based on observations with the Green Bank Telescope (GBT). However, we noted that due to the large GBT beam, it is possible that H I absorption against the background source is filled-in by emission from elsewhere in the galaxy. The GBT spectra obtained by B11 are shown

TABLE 2
TARGETED GALAXY-QUASAR PAIRS.

#	B11# ^a	Foreground Galaxy	Redshift	Background Radio Source	S_{FIRST} (mJy)	ρ (kpc)	$\Sigma_{\text{SFR}}^{\text{b}}$ ($M_{\odot} \text{ yr}^{-1} \text{ kpc}^{-2}$)
1	12	J122115.22+454843.2 ^c	0.0015	122105.480+454838.80	53.69	3.3	-
2	13	"	"	122106.854+454852.16	21.46	2.8	$< 3.46 \times 10^{-4}$
3	14	"	"	122107.811+454908.02	12.82	2.6	-
4	21	J141629.25+372120.4	0.0341	141631.039+372203.01	30.71	32.4	$< 2.34 \times 10^{-4}$
5	22	"	"	141630.672+372137.09	30.53	16.2	-
6	23	J160659.13+271642.6	0.0462	160658.315+271705.86	141.01	23.3	- ^d

^a Sightline I.D. from Borthakur et al. 2011

^b SFR estimated from $\text{H}\alpha$ emission towards the optical QSO using SDSS3 spectra.

^c Also known as UGC 7408

^d Measurements could not be made due to the presence of sky lines at the wavelength of $\text{H}\alpha$.

TABLE 4
HST COSMIC ORIGINS SPECTROGRAPH FOLLOW-UP
OBSERVATIONS OF UV-BRIGHT BACKGROUND QSOs.

Field	Program ID	Grating ^a	Exposure (s)
J104257.58+074850.5	12467	G140L	2221
J122115.22+454843.2	12486	G130M	8085

^a The far-ultraviolet (FUV) detector of the COS is sensitive to wavelengths between 900 and 2150 Å and has medium-resolution ($R \sim 20,000$) and low-resolution ($R \sim 3,000$) gratings.

in Figure 1. These single dish data were obtained using ON-OFF position switching mode. Therefore, in order to confirm the absence of absorption, we conducted follow-up observations with the Karl G. Jansky Very Large Array (VLA) of the NRAO¹ in B-configuration. These new observations provide almost two orders of magnitude higher spatial resolution than the GBT. In addition, we also obtained Hubble Space Telescope (HST) ultraviolet (UV) spectra of the background quasi-stellar objects (QSOs) in order to get an independent measurement of H I column density.

We proceed by describing our targets, followed by details of the observations and data analysis in Section 2. The results and a discussion on the implications of the findings are presented in Section 3. Finally, we conclude in Section 4 and comment on the potential of similar studies with upcoming facilities in the future. The cosmological parameters used in this study are $H_0 = 70 \text{ km s}^{-1} \text{ Mpc}^{-1}$, $\Omega_m = 0.3$, and $\Omega_{\Lambda} = 0.7$.

2. OBSERVATION

2.1. Targets

2.1.1. Targets for High Spatial Resolution 21 cm HI Imaging with the VLA

We carried out follow up VLA observations of three galaxies with radio bright background sources. Properties of the target galaxies such as their redshifts, stellar and H I masses, central metallicities, H I velocity centroids and widths are provided in Table 1. The GBT spectrum of the three galaxies obtained by B11 shows

strong H I emission. The measured H I masses indicate that these galaxies have more H I than stars. Based on the H I mass to disk size relationship derived by Swaters et al. (2002), these galaxies are expected to have extended H I disks well beyond their optical disks.

These three galaxies are probed by six sightlines corresponding to six radio bright background sources. Information on each of the sightlines including their IDs from the study by B11, position of the background radio sources, their 20 cm fluxes, and impact parameters are provided in Table 2. Three of the sightlines are QSOs with optical spectroscopic data from the Sloan Digital Sky Survey (SDSS). The non-detection of any $\text{H}\alpha$ in emission at the redshift of the foreground galaxy in the QSO spectra provides us with an upper limit on the star formation rate surface density (Σ_{SFR}).

Since all the galaxies were found to have strong 21 cm H I emission in the GBT spectra, it is impossible to rule out absorption being filled-in by emission from a different spatial location. Hence, we carried out high spatial resolution VLA observations to confirm the non-detections at the location of the background radio sources. The VLA in B-configuration is most appropriate for such a study as the size of the synthesized beam ($\sim 8'' \times 6''$) matches the extent of the background continuum sources and is hence most conducive to detecting absorption features. For example, the spatial resolution achieved in our imaging (column 6 of Table 3) is better than that prescribed by Dickey et al. (2000, resolution of $< 10''$) for extragalactic sources.

2.1.2. Targets for Follow-up Ultraviolet Spectroscopy with the HST

¹ The National Radio Astronomy Observatory is a facility of the National Science Foundation operated under cooperative agreement by Associated Universities, Inc.

TABLE 3
DESCRIPTION OF VLA OBSERVATIONS AND THE DATA PRODUCTS.

Field	Duration (hrs)	Bandwidth (MHz)	Bandwidth (km s ⁻¹)	Channel Width (km s ⁻¹)	Beam Size ^a (arcsec×arcsec)	$\sigma_{channel}$ (mJy/beam)	$\sigma_{cont.map}$ ^b (mJy/beam)
J122115.22+454843.2 ^c	2.0	1.0	211	0.8	7.45×5.58	3.06	0.292
J141629.25+372120.4	8.0	2.0	436	1.7	7.13×5.22	1.0	0.078
J160659.13+271642.6	8.0	4.0	883	3.4	8.35×5.94	0.9	0.102

^a Reported for the line image. The variation in beam size between continuum and the line image is less than 10%.

^b Average of all channel.

^c Also known as UGC 7408.

We obtained UV spectra for two of the QSO sightlines from our original sample that had confirmed 21 cm absorbers. The purpose of these observations was to detect and measure the Lyman α ($\lambda 1215.670$ Å) transition associated with the 21 cm absorbers and hence provide a measure of the H I column density independent of any assumption regarding the spin-temperature of the gas. The combination of H I absorption properties from the 21 cm hyperfine transition and the Lyman α transition can be used to measure the column density and spin temperature of the absorber simultaneously. The QSOs were observed with the Cosmic Origins Spectrograph (COS) aboard the HST under programs 12467 and 12486. One of the sightlines, SDSS J122115.22+454843.2, is the optical/UV counterpart of the radio sightline #2 (see Table 1). The other sightline is towards SDSS J104257.58+074850.5 probing galaxy GQ1042+0747 at an impact parameter of 1.7 kpc (Borthakur et al. 2010). The setups for the HST observations are presented in Table 4.

Unfortunately, the COS spectra for both the targets had insufficient flux at the rest-frame wavelength of Lyman α for the targeted galaxies. As a result no measurements could be made. The drop in UV flux of the QSOs is consistent with the presence of Lyman Limit Systems (LLS) at higher redshift towards these sightlines that have consumed most of the flux at shorter wavelengths. Therefore, for the remainder of the paper, we concentrate on the analysis and results from the 21 cm follow-up observations.

2.2. Data Acquisition and Analysis

2.2.1. Very Large Array Observations

We carried out a total of 18 hours of observations with the VLA in B-configuration under program 10C-120. We observed the field towards SDSS J122115.22+454843.2 (UGC 7408 hereafter) for 2 hours and the fields towards SDSS J141629.25+372120.4 (J141629 hereafter) and SDSS J160659.13+271642.6 (J160659 hereafter) for 8 hours each. The observations were carried out in dual polarization mode with a total bandwidth of 1, 2, and 4 Megahertz (MHz), respectively. This setup was chosen to yield velocity coverage of 211, 436, and 883 km s⁻¹ respectively. The VLA correlator, WIDAR, was set up to deliver 256 spectral channels for each of the used bandwidths, resulting in a velocity width of 0.8, 1.7, and 3.5 km s⁻¹ per channel, respectively. WIDAR being an XF correlator, the frequency resolution of the raw (unbinned and unsmoothed) spectra is 1.2 times the channel width (Rots 1982).

The data were reduced and calibrated following the

standard VLA calibration and imaging procedures using the Common Astronomy Software Applications package (CASA). The data were imaged using a “natural” weighting scheme for spectral line images. The natural weighting was preferred as it offered the highest possible signal to noise ratio in the images. Details of the observations and data products are provided in Table 3.

2.2.2. Existing Very Large Array Data

We also present existing VLA D-configuration data that were obtained under legacy I.D. AY190 and were first published by B11. The data were obtained in 2008 in dual polarization mode with a bandwidth of 1.5 MHz and 128 spectral channels using the old VLA correlator. These correspond to a velocity coverage of 330 km s⁻¹ and a channel width of 2.6 km s⁻¹, respectively. The data were reduced and calibrated following the standard calibration and imaging procedures using NRAO’s Astronomical Image Processing Software (AIPS). The spatial resolution achieved with the uniform weighting of the data is $52.''17 \times 38.''11$, which is not enough to resolve the background radio source into three individual sources. And hence, detailed spatial information on the associated H I absorption could not be made with these data, thus requiring the need for higher spatial and spectral resolution B-configuration data.

3. RESULTS AND DISCUSSION

In this section we present the continuum images and H I spectra from our VLA observations. Figures 2-4 show 21 cm radio continuum images overlaid as red contours on the SDSS r-band images in greyscale. Figure 2 also shows the VLA D-configuration H I emission map overlaid as yellow contours (first published by B11). The flux density measured for each of the background radio sources (continuum) is provided in column 4 of Table 1. Spectra extracted from each of the sightlines are shown in black on the right panels. The standard deviation in flux density per channel is plotted green. The errors are plotted in negative units (i.e. -1σ) for easy in visual identification of significant absorption features.

3.1. Cold Gas in UGC 7408

We detected a narrow absorption feature associated with UGC 7408 in our VLA B-configuration spectra towards sightline #2. The absorption feature peaks at a velocity of 444.5 km s⁻¹ and was measured to have a full-width at half maximum (FWHM) of 1.1 km s⁻¹. The width of the feature is comparable with our spectral resolution. No significant absorption features were seen towards sightlines #1 and #3.

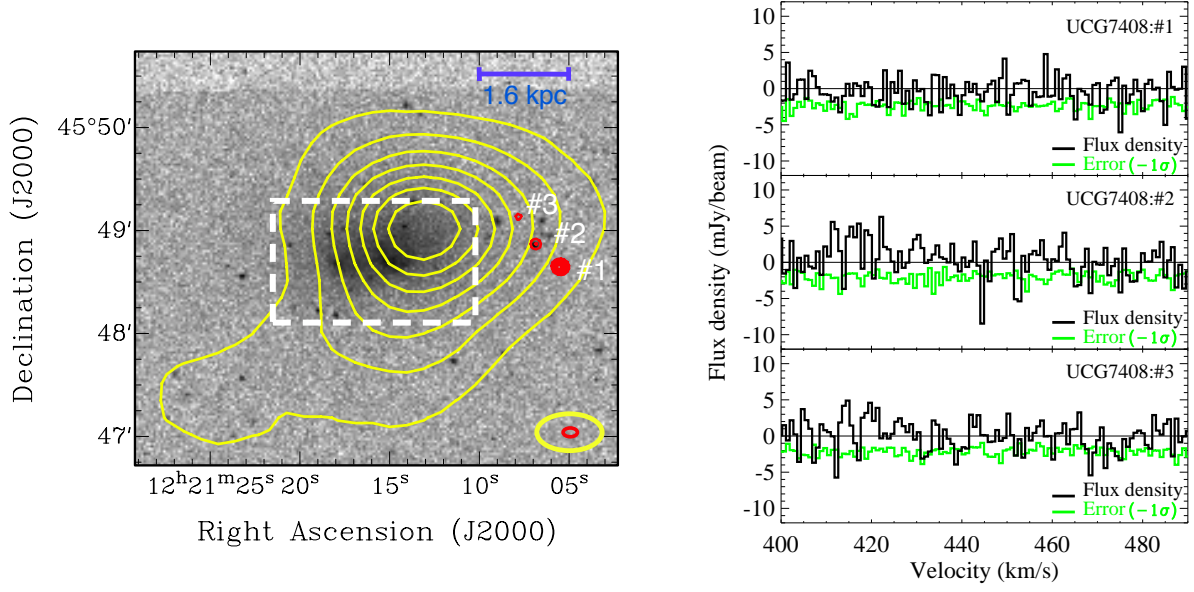


FIG. 2.— Left: SDSS r-band image of UCG 7408 in grayscale with VLA B-configuration continuum map and VLA D-configuration HI map (B11) shown as contours in red and yellow, respectively. The target galaxy, UCG 7408, is marked with a dashed white rectangle and the sightlines are labeled. The red contours show VLA B-configuration continuum map with flux levels of 10, 20, 30, 40, and 50 mJy/beam. The VLA D-configuration HI 21 cm column density are shown in yellows at levels corresponding to 7.2, 14.4, 21.6, 28.8, 36.0, 43.2, and $50.4 \times 10^{19} \text{ cm}^{-2}$, respectively. The synthesized beam for the D-configuration map ($67''.51 \times 45''.31$) is shown in yellow and that of the B-configuration is shown in red at the bottom right corner. Right: Spectra extracted at the position of the background sources (sightlines # 1, 2, and 3) are presented on the right panel. The errors in the measurements corresponding to standard deviation in flux density for each of the channel maps, derived using the imaging package in CASA, are shown in green. The errors are plotted in negative units (i.e. -1σ) for easy in visually estimating the strength of absorption features. A single pixel feature was detected in the spectrum towards sightline 2 at a velocity of 444.5 km s^{-1} . The spatial map of the HI in absorption is presented in the Figure 6. We do not see any absorption feature at strength 3σ or higher towards the other two sightlines probing the HI disk of UCG 7408.

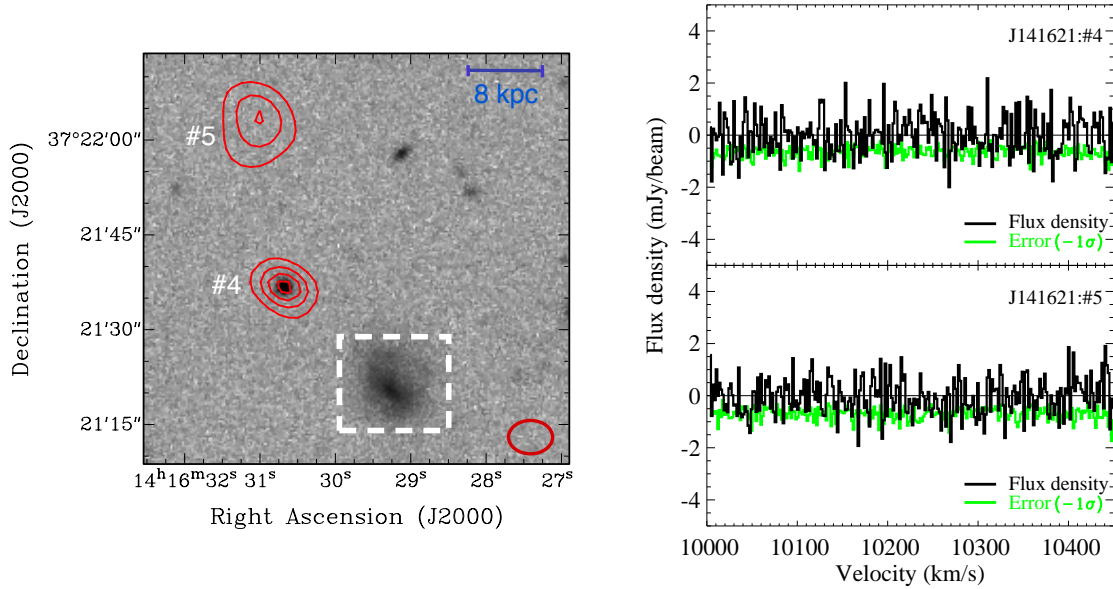


FIG. 3.— Left: SDSS r-band image of SDSS J141629.25+372120.4 in grayscale overlaid with contours of VLA B-configuration continuum map shown in red. The target galaxy, J141629, is marked with a dashed rectangle in white and the sightlines are labeled. The red contours are at flux levels of 5, 10, 15 and 20 mJy/beam. The beam is shown at the bottom right corner in red and the physical scale at the restframe of the target galaxy is shown on the top right-hand corner. Right: Spectra extracted at the position of the background sources (sightlines # 4 and 5) are presented in the right panel. The standard deviation in flux density (-1σ) in each of the channel maps are plotted in green. We do not see any absorption feature at strength 3σ or higher for both the sightlines.

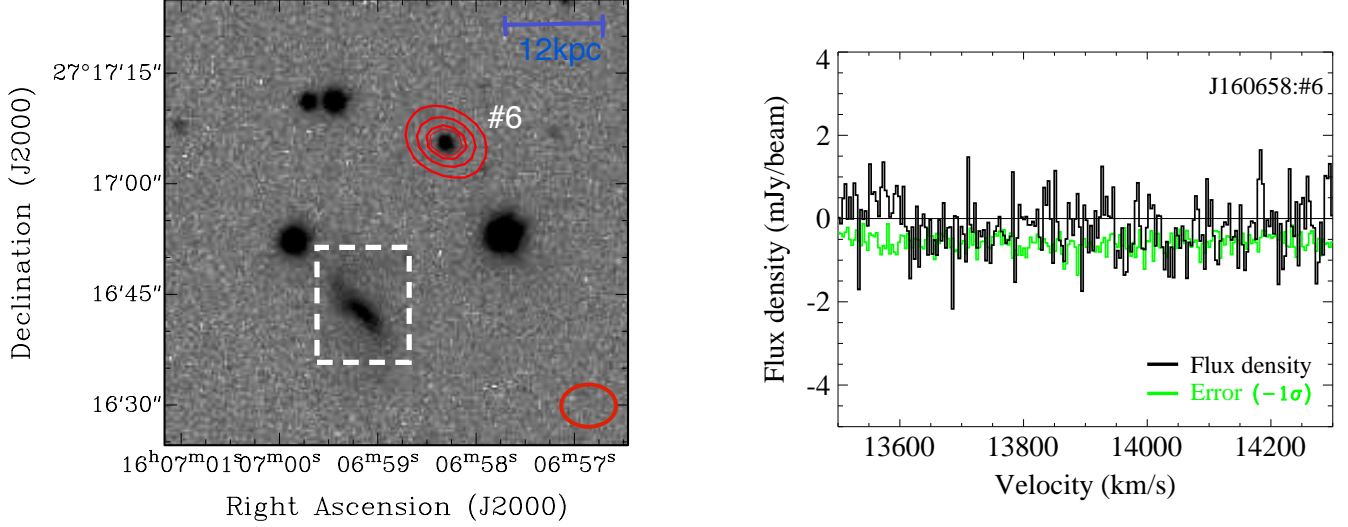


FIG. 4.— Left: SDSS r-band image of SDSS J160659.13+271642.6 in grayscale overlaid with contours of VLA B-configuration continuum map shown in red. The target galaxy, J160659, is marked with a dashed rectangle in white and the sightlines are labeled. The red contours are at flux levels of 50, 100, 150 and 170 mJy/beam. The VLA beam is shown at the bottom right corner in red and the physical scale at the rest-frame of the target galaxy is shown on the top right-hand corner. Right: Spectrum extract at the position of the background sources (sightline # 6) is presented on the right panel. The standard deviation in flux density (-1σ) in the channel maps is plotted in green. We do not see any absorption feature at strengths 3σ or higher towards this sightline. This being the background source with the largest integrated flux among the six sightlines discussed in this paper, we estimate the most stringent optical depth limit of $\tau_{\#6} \leq 0.03$ for this target.

TABLE 5
OPTICAL DEPTH AND COLUMN DENSITY MEASUREMENTS.

#	Background Radio Source	ρ (kpc)	$S_{1.4 \text{ GHz}}$ (mJy)	$\sigma_{4 \text{ km/s}}$ mJy	Abs strength (mJy)	$\tau_{3\sigma}$	$N(\text{HI})_{3\sigma}^a$ ($\times 10^{19} \text{ cm}^{-2}$)
1	122105.480+454838.80	3.3	65.18	1.42	<4.26	<0.07	< 2.55
2	122106.854+454852.16	2.8	24.72	1.42	-	-	-
2 ^b	122106.854+454852.16 ^b	2.8	13.98	-	10.41 ^c	1.39 ^c	6.47
3	122107.811+454908.02	2.6	13.44	1.42	<4.26	<0.39	<14.22
4	141630.672+372137.09	16.2	32.79	0.65	<1.96	<0.06	<2.19
5	141631.039+372203.01	32.4	25.30	0.65	<1.96	<0.08	<2.92
6	160658.315+271705.86	23.3	190.17	0.83	<2.49	<0.01	<0.36

^a Assuming a line width of 4 km s^{-1} , a spin temperature $T_s = 50 \text{ K}$, and a covering fraction, $f = 1$.

^b Region where the absorption was detected (see Figure 2 for details).

^c At the intrinsic resolution of the data (channel width of 0.84 km s^{-1}).

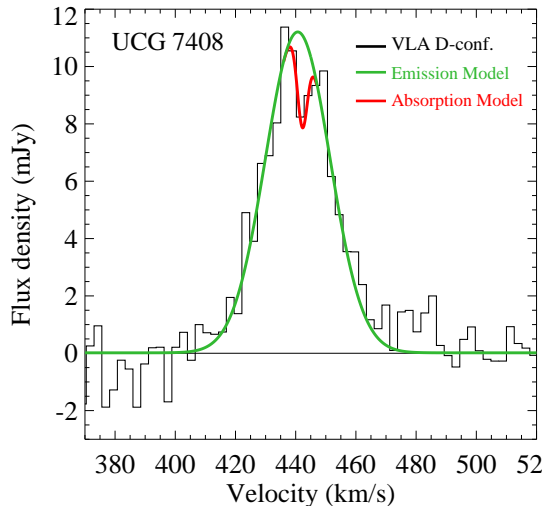


FIG. 5.— VLA D-configuration HI spectrum extracted from a region the size of the synthesized beam centered at the quasar (first published by B11). The data show a Gaussian HI emission feature with an absorption feature ($\text{FWHM}=4.75 \text{ km s}^{-1}$) superimposed at the peak of emission. B11 concluded that the broad Gaussian emission feature was produced by the atomic gas that filled-in the beam, whereas the gas towards the quasar sightline, covering only a small fraction of the beam, produced the superimposed absorption.

Previously, B11 had found an HI absorption feature associated with UGC 7408 towards the background quasar encompassing sightlines # 1, 2, and 3. The absorption was found as dip on an otherwise Gaussian emission profile. The VLA D-configuration spectrum extracted from a region the size of the synthesized beam centered at the quasar is shown in Figure 5. B11 concluded that the atomic gas that filled-in the beam contributed to the broad Gaussian emission feature, whereas the gas towards the quasar sightline, covering a small fraction of the D-configuration beam, produced the superimposed absorption. By subtracting the emission, as modeled by a Gaussian profile, these authors found the absorption feature to have a FWHM of 4.75 km s^{-1} at the spectral resolution of 3.1 km s^{-1} corresponding to a channel width 2.6 km s^{-1} (Rots 1982). The feature peaked at 442.2 km s^{-1} . It is worth noting that the velocity centroid of the absorption feature is likely to be effected by errors in modeling the intrinsic emission. For example, any deviation from a Gaussian emission profile would introduce a spurious offset.

Our 21cm absorber towards sightline #2 is consistent with the superimposed absorption feature detected by B11. The offset in the velocity centroids between the two detections is consistent with the difference in the spectral resolution between the two data sets (a factor of ~ 2.5). This is also supported by the fact that the two absorption features have similar strengths that differ by less than 8%. The HI absorber detected in the D-configuration is broader and shallower than that detected in B-configuration. Therefore, the D-configuration data are consistent with lower spectral resolution observations of an intrinsically narrow and deep absorption feature such as the one detected in B-configuration. While the two detections are consistent, the narrowness of the absorber clearly demonstrates the need for higher spectral resolution to obtain precise constraints on the physical conditions and kinematics of 21 cm absorbers.

Similar narrow HI features have been detected in absorption in the Large Magellanic Cloud (LMC) (1.4 km s^{-1} by Dickey et al. 1994), and Small Magellanic Cloud (SMC) (1.2 km s^{-1} by Dickey et al. 2000). However, until recently most of the extragalactic HI absorption surveys, owing to their low spectral resolution, detected only absorbers with large widths. Therefore, it is possible that these studies might have missed absorbers such as this.

3.1.1. Covering Fraction of Cold Gas in UGC 7408

We present the HI map from the channel corresponding to the velocity of the absorption feature (444.5 km s^{-1}) seen towards sightline #2 in Figure 6. The background radio source is shown in black contours. The map is color coded to show absorption in blue, noise ($\pm 1\sigma$) in green, and emission in yellow/red. However, unlike emission, HI absorption can only be measured in the region covered by the background radio source.

Absorption associated with sightline #2 can be seen in blue in Figure 6, covering the Northeast quadrant of the background source. The physical size (area) of the HI cloud responsible for the absorption is $\sim 0.04 \text{ kpc}^2$. The implied covering fraction, f , of the background source by the cloud is $\approx 25 - 30\%$.

3.1.2. Physical Properties of the HI Absorber

A spectrum extracted from the position of the absorber (identified as a white oval of same size as the beam) is shown on the right. We measured the peak depth in flux density for the feature to be 10.41 mJy . For comparison, we also present in Figure 6 the D-configuration absorption spectrum that was obtained by subtracting the HI emission model from the spectrum in Figure 5. The region of the galaxy from which the D-configuration spectrum was extracted is shown as the white dashed rectangle on the image in the left panel of Figure 6. As noted earlier, the absorption feature seen in the B-configuration data is deeper and narrower than that seen in the VLA D-configuration data. The B-configuration data have higher spectral and spatial resolution, however they have lower signal to noise ratio than the D-configuration data. Nevertheless, the feature was confirmed at $> 5\sigma$ at that channel or at $> 3\sigma_{\text{average}}$, the average noise over all channel.

From our B-configuration data, we estimated the peak optical depth of this absorber to 1.37 using the following relation

$$\tau = -\ln\left(\frac{I_o - I_{abs}}{I_o}\right) \quad (1)$$

where I_o is the flux density of the background quasar at the position of the absorber of 13.98 mJy (see Figure 6 left panel) and I_{abs} is the peak strength of the absorption feature of 10.41 mJy . If we assume the width of the line is due to collisional excitation of the hydrogen atoms, we can relate the kinetic temperature of the gas to the width of the line as

$$T_k \leq 21.855 (\Delta v)^2 \quad (2)$$

where Δv is the FWHM of the line in km s^{-1} . In this case, $\Delta v = 1.1 \text{ km s}^{-1}$ and implies a kinetic temperature, $T_k \leq 26.4 \text{ K}$. This indicates that the temperature

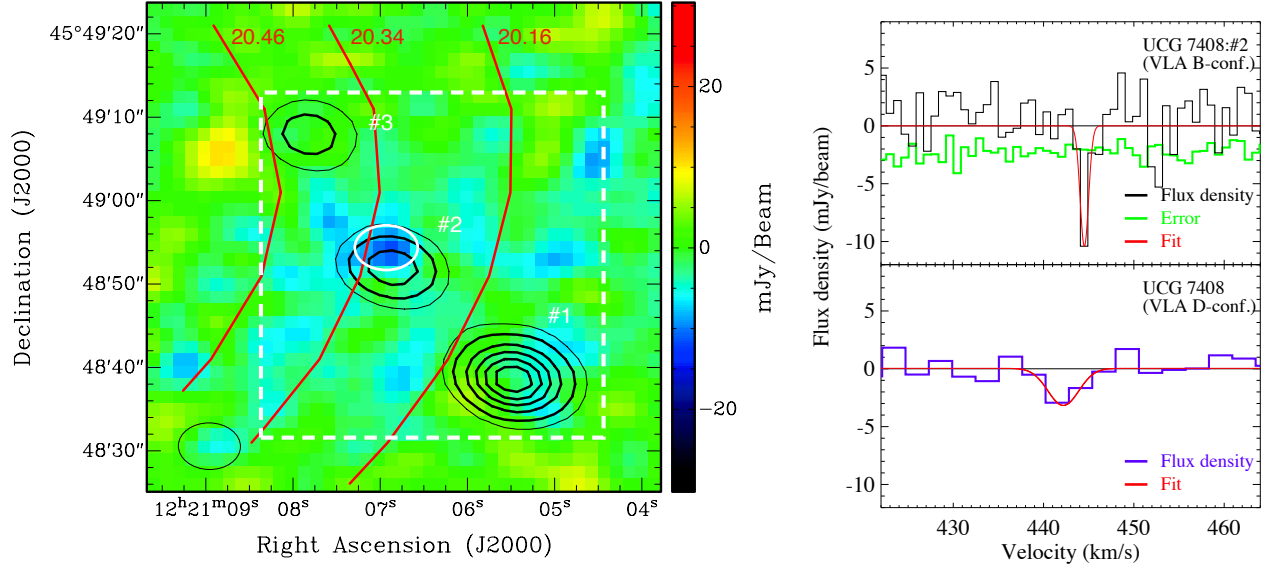


FIG. 6.— Left: 21 cm HI absorption map of UGC 7408 corresponding to the channel at velocity, $v = 444.5 \text{ km s}^{-1}$. The colors show the observed flux densities such that blue represents pixels with negative flux density i.e. **absorption**, yellow/red represents pixels with positive flux density i.e. **emission**, and green indicate pixels within the observed **noise** ($\pm 1\sigma$) in the data. The background source is shown in black contours at flux density levels of 5, 10, 20, 30, 40, and 50 mJy/beam. It is worth noting that we are sensitive to absorption only against the background radio source. However, we are sensitive to emission in the entire region. The synthesized beam size ($\approx 230 \text{ pc} \times 173 \text{ pc}$ in physical units) is shown in the lower left-hand corner. The red contours show the VLA D-configuration HI emission map with contour levels indicating 14.4 , 21.7 , and $28.9 \times 10^{19} \text{ cm}^{-2}$. Spectra extracted from the regions marked in white are shown in the right panel. Right: VLA B-configuration HI spectrum extracted from the region marked in the white oval, the size of the beam, is shown in the top panel in black. The absorption has a peak depth of 10.41 mJy and the flux density of the background source at the same region is 13.98 mJy . The absorption feature is unresolved and the limiting FWHM of was measured to be 1.1 km s^{-1} . This corresponds to a kinetic temperature, $T_k \leq 26 \text{ K}$. The VLA-D configuration HI spectrum extracted from the white dashed rectangular region (similar in size to the D-configuration beam) is shown in the lower panel in blue. The feature has a FWHM of 4.75 km s^{-1} and a centroid at 442.2 km s^{-1} . The absorption spectrum was obtained by subtracting out the Gaussian emission profile from the raw spectrum as discussed in detail by B11.

of this absorber is similar to that observed in cold neutral medium (CNM) of the LMC and SMC (Dickey et al. 1994, 2000).

Assuming the kinetic temperature as a proxy for spin temperature (i.e. $T_k = T_s = 26.4 \text{ K}$), we estimate the column density of H I in this absorber to be $6.3 \times 10^{19} \text{ cm}^{-2}$ using the following expression

$$N(\text{H I}) = 1.823 \times 10^{18} \frac{T_s}{f} \int \tau(v) dv \text{ cm}^{-2}, \quad (3)$$

where $\tau(v)$ is the 21 cm optical depth as a function of velocity in km s^{-1} . From the Gaussian fit to the absorber, we estimate $\int \tau(v) dv = 1.3$. In this case, the covering fraction is unity, $f = 1$, as we are measuring optical depth, $\tau(v)$, at the region of the background source where the absorber was detected.

The column density of cold gas as derived from the absorption feature is significantly lower than the total H I column density seen in emission. By comparing the two, we find that the ratio of cold-to-total H I column density associated with the absorber to be $\approx 30\%$. Folding in the covering fraction, we find that only $\approx 10\%$ of the total H I by mass exists in the cold phase. The non-detections of H I in absorption towards sightlines 1 and 3 provide upper limits on the column densities of 2.9 and $14.2 \times 10^{19} \text{ cm}^{-2}$ respectively. The same exercise of comparing these column densities to that observed in emission implies that the cold-to-total H I towards sightlines 1 and 3 are $\lesssim 20\%$ and $\lesssim 50\%$, respectively.

3.1.3. Nature of HI in UGC 7408

Our results suggest that the process of condensation is suppressed in UGC 7408. We found that a large fraction of atomic gas in the extended disk of this galaxy is warm with temperature much larger than a few 100 K . Therefore, we conclude that most of the atomic gas in the extended disk of UGC 7408 failed to condense into the atomic gas clouds of $100\text{--}50 \text{ K}$ (typically found in the Milky Way ISM). We did detect a small fraction of gas in the cold phase with temperature $\sim 25 \text{ K}$. This is much lower than the temperatures commonly seen in the CNM of the Milky Way (Heiles & Troland 2003; Strasser et al. 2007). In fact, at such low temperatures most of the gas in the Milky Way is in the molecular phase. The existence of such cold atomic gas suggests that the fraction of H I that was able to condense into the cold phase remained in the atomic state and avoided the transition to molecular phase.

The atomic hydrogen in the SMC also exhibits very similar properties. For instance, Dickey et al. found that less than 15% of the total H I in the SMC is in the cold-phase. They also found the temperature of cold phase to be typically 40 K or less. They suggested that the difference in the properties of the CNM between the SMC and the Milky Way is a consequence of the difference in the metallicity in the ISM. Low-metallicity implies lower radiative cooling. In particular for clouds where cooling is dominated by fine-structure line emission, the thermal equilibrium between the warm and the cold phase re-

quires higher pressures with decreasing metal abundance (Wolfire et al. 1995). This limits the existence of cold clouds to region of higher pressure, and hence the reduction in the cold gas fraction. Similar effects are observed in DLAs where the spin temperatures are inversely proportional to the metallicity of the DLA (Kanevar et al. 2009). Again, this emphasizes the inefficient cooling of gas at lower metallicities.

On the other hand, the lower metallicity would imply lower dust content and therefore, the fraction of atomic gas that is able to cool does not suffer from photoelectric heating by dust grains. However, the lack of dust grains is likely to impede the production of molecules. Dust plays a crucial role in shielding gas clouds against ionization thus aiding in atomic-to-molecular transition. Therefore, a drop in metallicity/dust content requires a much larger column of neutral gas to shield the clouds and form molecules (see Fig.1 in Krumholz et al. 2009). Observationally, this is evident from the variation in the minimum neutral gas column densities required to detect molecules in galaxies as a function of metallicity. For example, in the Milky Way the transition occurs when the neutral gas column density is $10^{20.7} \text{ cm}^{-2}$ or higher (Savage et al. 1977). The same for LMC and SMC was found to be at $N(\text{HI}) > 10^{21.3} \text{ cm}^{-2}$ and $> 10^{22.0} \text{ cm}^{-2}$ respectively (Tumlinson et al. 2002).

Therefore, it is likely that UGC 7408 has a very low molecular gas fraction as compared to its neutral gas content. This would explain the small physical extent of the stellar component in this galaxy unlike its extended H I distribution as well as the suppression in star formation (as indicated by the limiting star formation rate surface density in Table 1) at the position of the absorber despite its low temperature.

3.2. Extended H I Disks of J141629 and J160659

We did not detect any H I absorbers toward the sightlines 4 and 5 probing galaxy J141629 at impact parameters of 16.2 and 32.4 kpc and sightline 6 probing galaxy J160659 at an impact parameter of 23.3 kpc. The limiting optical depths and column densities estimated from 3σ noise in the spectra are presented in Table 5.

Both these galaxies have large H I reservoirs ($\text{Log}[M_{\text{HI}}] = 9.4$ and 9.9 respectively) and hence are expected to have extended H I distributions. The empirical H I mass to size relationship derived for dwarf galaxies from the WHISP Survey (Swaters et al. 2002) predicts that the H I distribution in J141629 and J160659 have radii, R_{HI} , of 15.3 and 30.1 kpc, respectively. This implies that J160659 is probed by sightline #6 ($\rho = 23.3$ kpc) within the $R_{\text{HI}} = 30.1$ kpc. However, no H I was observed in absorption. The 3σ limit on the absorption column density towards this sightline is $3.6 \times 10^{18} \text{ cm}^{-2}$. But, the expected H I surface density within R_{HI} is $\geq 1 \text{ M}_{\odot} \text{ pc}^{-2}$, which is equivalent to a column density of $\geq 1.3 \times 10^{20} \text{ cm}^{-2}$. This implies that the limiting column density is 35 times lower than the column density predicted at R_{HI} . Similarly, sightline #5 probes J141629 at the edge of its H I disk ($\rho = 16.2$ kpc and $R_{\text{HI}} = 15.3$ kpc) and the upper limit on its H I column places it an order of magnitude below that expected at R_{HI} . This suggest that cold-to-average H I column densities could be lower than 10% towards these sightlines. A similar argument based on the empirically observed ra-

tio between H I to optical radius of ~ 3 for dwarf galaxies also implies an unusually low cold H I ($T \sim 100$ K or less) content at the position of these sightlines.

There could be two likely causes for the non-detection of H I in these sightlines. The first possibility is that the H I distribution is highly patchy and the covering fraction of gas with column density $\sim 10^{20} \text{ cm}^{-2}$ is significantly smaller than 1. If that were the case, then it would also imply that true column density of the patchy H I is much higher than $1.3 \times 10^{20} \text{ cm}^{-2}$ within R_{HI} . The second possibility is that the atomic gas is warm ($T_{\text{spin}} > 1000$ K) and produces a broad (due to Doppler broadening) and shallow (i.e. low optical depth because $T_{\text{spin}} \propto (\tau)^{-2/3}$; see Eq. 5 from B11) absorption feature. Such features would remain hidden in our data due to the limited signal to noise ratio. This is a disadvantage that impacts most 21 cm absorption studies.

4. CONCLUSION

We presented follow-up VLA B-configuration observations of six quasar sightlines from the GBT 21cm H I absorption sample of B11. The sightlines probed three foreground galaxies. This includes three sightlines probing dwarf galaxy, UGC 7408. Strong H I emission was detected towards these sightlines in the GBT spectra and hence a reliable limit on the optical depth based on the non-detection of absorption could not be made. Therefore, we obtained high spatial resolution imaging with the VLA and found the following:

1. A narrow H I absorber was detected towards sightline J122106.854+454852.16 (#2) at 444.5 km s^{-1} . The absorber is associated with the extended H I disk of UGC 7408 at an impact parameter of 2.8 kpc. This absorber was tentatively detected by B11 in their low spatial and spectral resolution VLA D-configuration data. Our higher resolution data showed the absorber to be narrow and unresolved. A Gaussian fit to our data gives a FWHM of 1.1 km s^{-1} and a corresponding kinetic temperature of $T_k \approx 26$ K. Assuming the kinetic temperature as a proxy for the spin temperature, we estimated the column density of the absorber to be $6.3 \times 10^{19} \text{ cm}^{-2}$.
2. The area of the cloud associated with the absorber was measured to be 0.04 kpc^2 . This implies a covering fraction of the background source $\sim 25\text{-}30\%$.
3. The cold-to-total H I column density in the absorbing cloud towards this sightline was estimated to be $\sim 30\%$. In terms of mass, the cold phase is about $\sim 10\%$ of the total H I.
4. The low fraction of cold-to-total H I and the existence of cold H I at extremely low temperatures, where gas normally transitions to molecular phase, suggests that the process of condensation is suppressed in this galaxy. The likely explanation for the suppression is the low metal content in this galaxy. Similar properties of the CNM were seen in the SMC. Together, these two cases are consistent with the effects of low-metallicity in suppressing condensation.

5. We reported non-detection of H I in absorption for the remaining five sightlines. The limiting optical depths range from $\tau \leq 0.01$ -0.39. These limits are about three times better than those measured by B11 towards most sightlines.
6. One of the sightlines is expected to probe the extended H I disk ($\rho < R_{\text{HI}}$) of the foreground galaxy J160659.13+271642.6. The non-detection of H I in absorption towards that sightline indicates an extremely low column density of cold gas ($T_{\text{spin}} \lesssim 100$ K). Two likely interpretations are that either the cold gas distribution is highly patchy or the H I is at much higher temperature ($T_{\text{spin}} > 1000$ K).
7. The non-detection of H I puts stringent limits on H I optical depth. This lends support to the conclusions from the B11 survey that the covering fraction of cold gas at column densities greater than that of DLA is very small beyond ≈ 15 kpc.

Based on our results, we emphasize the need for a statistically larger sample to probe gas within 20 kpc of galaxies. Currently, plans are underway for two such surveys - the First Large Absorption Survey in HI (FLASH; P.I. Sadler; Allison et al. 2012) with the Australian Square Kilometre Array Pathfinder (ASKAP) and the MeerKAT Absorption Line Survey (P.Is. Gupta & Srianand) with the South African MeerKAT radio telescope. Both of them are pathfinder missions for the Square Kilometer Array (SKA). The high sensitivity of SKA will make it the ideal telescope for mapping cold gas in absorption against fainter background sources. These upcoming facilities and the planned surveys promise to substantially improve our understanding of small-scale properties of cold gas as a function of radial distance within their host galaxies. A large sample will also facilitate a census of variations in cold-gas properties and the process of condensation as a function of galaxy properties such as stellar mass, gas content, metallicity, SFR etc. That will be the crucial step in understanding the physics behind the

process of condensation, its regulation, and how that translates to evolution of galaxies across the full stellar mass spectrum.

Acknowledgements

This manuscript has benefited from insightful suggestions and comments from the referee. We also thank M. Livio and L. Blitz for useful discussions. We thank the staff of the Very Large Array for help during the data acquisition and reduction. SB acknowledges financial support from HST grant 12467² and from NRAO to cover travel and lodging during the data reduction under program 10C-120 at the Pete V. Domenici Science Operations Center (SOC). TMT appreciates support for this work from NSF grant AST0908334.

Funding for the SDSS and SDSS-II has been provided by the Alfred P. Sloan Foundation, the Participating Institutions, the National Science Foundation, the U.S. Department of Energy, the National Aeronautics and Space Administration, the Japanese Monbukagakusho, the Max Planck Society, and the Higher Education Funding Council for England. The SDSS Web Site is <http://www.sdss.org/>. The SDSS is managed by the Astrophysical Research Consortium for the Participating Institutions. The Participating Institutions are the American Museum of Natural History, Astrophysical Institute Potsdam, University of Basel, University of Cambridge, Case Western Reserve University, University of Chicago, Drexel University, Fermilab, the Institute for Advanced Study, the Japan Participation Group, Johns Hopkins University, the Joint Institute for Nuclear Astrophysics, the Kavli Institute for Particle Astrophysics and Cosmology, the Korean Scientist Group, the Chinese Academy of Sciences (LAMOST), Los Alamos National Laboratory, the Max-Planck-Institute for Astronomy (MPIA), the Max-Planck-Institute for Astrophysics (MPA), New Mexico State University, Ohio State University, University of Pittsburgh, University of Portsmouth, Princeton University, the United States Naval Observatory, and the University of Washington.

REFERENCES

- Allison, J. R., Curran, S. J., Emonts, B. H. C., et al. 2012, *MNRAS*, 423, 2601
- Birnboim, Y., & Dekel, A. 2003, *MNRAS*, 345, 349
- Bordoloi, R., Tumlinson, J., Werk, J. K., et al. 2014, *ArXiv e-prints*
- Borthakur, S., Heckman, T., Strickland, D., Wild, V., & Schiminovich, D. 2013, *ApJ*, 768, 18
- Borthakur, S., Tripp, T. M., Yun, M. S., et al. 2011, *ApJ*, 727, 52 (B11)
- . 2010, *ApJ*, 713, 131
- Darling, J., Giovanelli, R., Haynes, M. P., Bolatto, A. D., & Bower, G. C. 2004, *ApJ*, 613, L101
- Dickey, J. M., Mebold, U., Marx, M., et al. 1994, *A&A*, 289, 357
- Dickey, J. M., Mebold, U., Stanimirovic, S., & Staveley-Smith, L. 2000, *ApJ*, 536, 756
- Ford, A. B., Davé, R., Oppenheimer, B. D., et al. 2013, *ArXiv e-prints*
- Gupta, N., Srianand, R., Bowen, D. V., York, D. G., & Wadadekar, Y. 2010, *MNRAS*, 408, 849
- Gupta, N., Srianand, R., Noterdaeme, P., Petitjean, P., & Muzahid, S. 2013, *A&A*, 558, A84
- Gupta, N., Srianand, R., Petitjean, P., et al. 2007, *ApJ*, 654, L111
- Gupta, N., Srianand, R., Petitjean, P., Noterdaeme, P., & Saikia, D. J. 2009, *MNRAS*, 398, 201
- Heiles, C., & Troland, T. H. 2003, *ApJ*, 586, 1067
- Kacprzak, G. G., Churchill, C. W., Ceverino, D., et al. 2010, *ApJ*, 711, 533
- Kalberla, P. M. W., & Kerp, J. 2009, *ARA&A*, 47, 27
- Kanekar, N., & Chengalur, J. N. 1997, *MNRAS*, 292, 831
- Kanekar, N., Smette, A., Briggs, F. H., & Chengalur, J. N. 2009, *ApJ*, 705, L40
- Keeney, B. A., Momjian, E., Stocke, J. T., Carilli, C. L., & Tumlinson, J. 2005, *ApJ*, 622, 267
- Kennicutt, Jr., R. C., Lee, J. C., Funes, José G., S. J., Sakai, S., & Akiyama, S. 2008, *ApJS*, 178, 247
- Kereš, D., Katz, N., Weinberg, D. H., & Davé, R. 2005, *MNRAS*, 363, 2
- Krumholz, M. R., McKee, C. F., & Tumlinson, J. 2009, *ApJ*, 693, 216
- Lane, W. M., & Briggs, F. H. 2001, *ApJ*, 561, L27
- Maller, A. H., & Bullock, J. S. 2004, *MNRAS*, 355, 694
- Meiring, J. D., Tripp, T. M., Werk, J. K., et al. 2013, *ApJ*, 767, 49
- Pettini, M., & Pagel, B. E. J. 2004, *MNRAS*, 348, L59
- Prochaska, J. X., Weiner, B., Chen, H.-W., Mulchaey, J., & Cooke, K. 2011, *ApJ*, 740, 91
- Rots, A. 1982, in *Synthesis Mapping*, ed. A. R. Thompson & L. R. D’Addario, 8

- Savage, B. D., Bohlin, R. C., Drake, J. F., & Budich, W. 1977, *ApJ*, 216, 291
- Schaye, J., Carswell, R. F., & Kim, T.-S. 2007, *MNRAS*, 379, 1169
- Steidel, C. C., Kollmeier, J. A., Shapley, A. E., et al. 2002, *ApJ*, 570, 526
- Strasser, S. T., Dickey, J. M., Taylor, A. R., et al. 2007, *AJ*, 134, 2252
- Swaters, R. A., van Albada, T. S., van der Hulst, J. M., & Sancisi, R. 2002, *A&A*, 390, 829
- Tripp, T. M., Sembach, K. R., Bowen, D. V., et al. 2008, *ApJS*, 177, 39
- Tripp, T. M., Meiring, J. D., Prochaska, J. X., et al. 2011, *Science*, 334, 952
- Tumlinson, J., Shull, J. M., Rachford, B. L., et al. 2002, *ApJ*, 566, 857
- Tumlinson, J., Thom, C., Werk, J. K., et al. 2011, *Science*, 334, 948
- Vermeulen, R. C., Pihlström, Y. M., Tschager, W., et al. 2003, *A&A*, 404, 861
- Wakker, B. P., & Savage, B. D. 2009, *ApJS*, 182, 378
- Werk, J. K., Prochaska, J. X., Tumlinson, J., et al. 2014, *ApJ*, 792, 8
- Wolfire, M. G., Hollenbach, D., McKee, C. F., Tielens, A. G. G. M., & Bakes, E. L. O. 1995, *ApJ*, 443, 152